Hindawi
International Journal of Antennas and Propagation
Volume 2021, Article ID 6649439, 13 pages
https://doi.org/10.1155/2021/6649439

Research Article

Virtual Reconstruction-Based Robust Adaptive Beamforming for Distributed Digital Subarray Antennas

Jian Lu,[1] **Jian Yang**,[1] **Bo Hou**,[2] **Fengchao Zhu**,[2] **Zhiyong Yu**,[2] **and Guangbin Liu**[1]

[1]*School of Engineering, Rocket Force University of Engineering, Xi'an 710025, China*
[2]*School of Support, Rocket Force University of Engineering, Xi'an 710025, China*

Correspondence should be addressed to Jian Yang; yangjian@nudt.edu.cn

Received 24 October 2020; Revised 31 December 2020; Accepted 8 January 2021; Published 31 January 2021

Academic Editor: Giuseppina Monti

For the distributed digital subarray antennas (DDSA), the conventional beamforming may give rise to grating lobes, high sidelobes, and other problems. In this paper, the gaps between the subarrays are filled with virtual array elements, and then the DDSA can form a virtual contiguous array. More concretely, based on the direction-of-arrival (DOA) estimation of the signal sources, the interference components of the virtual elements and the interference-plus-noise covariance matrix (INCM) of the virtual contiguous array can be reconstructed. At low signal-to-noise ratio (SNR), the DOA estimation of the desired signal is implemented by subarray adaptive beamforming. Finally, with the steering vector of the desired signal and reconstructed INCM, the weight vector of the proposed beamformer can be obtained, which must be applied to the rearranged data matrix received by the actual and virtual elements. Simulation results are provided to demonstrate the effectiveness of the proposed algorithm.

1. Introduction

Compared with a single antenna, the distributed digital subarray antennas (DDSA) can provide better spatial resolution, wider beam coverage, and macro diversity gain [1]. The DDSA can work cooperatively as a single array, which significantly increases the output signal-to-interference-plus-noise ratio (SINR) and achieves ultralow sidelobe performance [2, 3]. Owing to these excellent advantages, the DDSA has received a lot of interest as a new leading-edge technology for radar [4–6], sonar [7], wireless communication [8–10], and other areas.

At present, there are some research results about the DDSA, which can be generally divided into two categories, i.e., direction-of-arrival (DOA) estimation and digital beamforming. In terms of DOA estimation, the long baseline separation technique in [11] was proposed to achieve superresolution direction finding. In [12, 13], the estimation of signal parameters via rotational invariance techniques-(ESPRIT-) based methods was applied to sparse arrays. In [14], by combining the multiple signal classification (MUSIC) algorithm with sparse subarrays, the closed-form eigenstructure-based DOA estimation was proposed to eliminate ambiguity. In [15], by combining virtual filling of the gaps between the subarrays with the modified matrix pencil method, the grating lobes were suppressed, and then the DOA of the desired signal can be accurately determined. In [16], the virtual elements between inside and outside the subarrays were constructed with different approaches, and then the superresolution DOA estimation was realized with sparse subarrays. In the aspect of beamforming, to reduce the parameters storage and computational load, the distributed and parallel subarray beamforming was proposed in [7]. The main characteristic of this method is to reduce the hardware resources, but the anti-interference performance is not significantly improved. In [4], a Fresnel-based frequency domain adaptive beamforming was proposed to eliminate the envelope migration problem. The research object of this method is the large aperture distributed array radar. However, due to the negligible envelope migration in the small DDSA system, this beamforming algorithm is not suitable. In [17], the distributed linearly constrained minimum variance (LCMV) beamformer was proposed to suppress interference and optimize the signal-to-noise ratio

(SNR), which greatly reduced the transmission requirements. But this method requires the accurate DOA of the desired signal in advance, especially at low SNR. In [6], a spatial multi-interference suppression method based on joint adaptive weight was proposed for the distributed array radar to improve the performance of the interference suppression in the case of massive sidelobe interferences. In addition to the DOA of the desired signal, this beamforming algorithm needs interference-plus-noise covariance matrix (INCM) reconstruction for each subarray, which greatly increases the computational complexity. In [5], a two-stage adaptive beamforming technique for distributed array radars was proposed to cancel multiple mainlobe and sidelobe jammings. However, this algorithm requires the full distributed array aperture to be sufficiently large. If not, the desired signal may be suppressed while cancelling the mainlobe jammings.

In this paper, the virtual filling technique is applied to the DDSA, and the gaps between the subarrays are filled with the virtual elements. By dividing the DDSA into two rotation-invariant subarray sets, the DOAs of the interfering signals can be accurately estimated, and the received data on the virtual elements can be reconstructed. Then, a virtual contiguous array can be formed, which significantly increases the degrees of freedom (DOF) of the proposed beamformer, and then a novel beamforming algorithm is devised based on the INCM reconstruction. In addition, to obtain the DOA of the desired signal at low SNR, we propose a DOA estimation method by estimating the subarray steering vector. After that, simulation results demonstrate the effectiveness of the proposed algorithm. Our main contributions are summarized as follows:

(1) We apply the ESPRIT-like method to DOA estimation of the incident signals by dividing the DDSA into two rotation-invariant subarray sets and estimate the DOA of the desired signal at low SNRs by solving the optimization problem.

(2) Based on the DOA estimation, we estimate the received interfering signals on the virtual elements and apply the data to the INCM reconstruction of the virtual contiguous array.

(3) We give the complete data treatment of the proposed beamforming involved in the weight vector and reconstructed sampling data set.

The remainder of this paper is organized as follows. In Section 2, the DDSA signal model and background are described. A robust adaptive beamforming based on virtual array elements and INCM reconstruction is proposed in Section 3. Simulation examples are provided in Section 4. Finally, some conclusions are drawn in Section 5.

2. DDSA Signal Model and Background

Consider a linear DDSA system of M identical subarrays, which belongs to the uniform linear array (ULA) of N omnidirectional sensors, with a half wavelength spacing d. As shown in Figure 1, the solid circles are actual elements, and the nonfilled circles are virtual sensors. The notch widths between the subarrays are $D_i = h_i d$ $(i = 1, 2, \ldots, M-1)$, where D_i is an integer multiple of the interelement spacing d. If the first sensor of subarray 1 is considered as the reference one of the whole antenna, the location of the n-th element in subarray m can be represented by $p(n,m)d$, where $p(n,m)$ is written as

$$p(n,m) = (m-1)N + n - 1 + \sum_{i=1}^{m-1} h_i, \quad n = 1, 2, \ldots, N, m = 1, 2, \ldots, M. \tag{1}$$

In Figure 1, there are $M-1$ virtual subarrays, and the location of the l-th element in virtual subarray m can be expressed as $q(l,m)d$, where $q(l,m)$ is represented by

$$q(l,m) = mN + l - 1 + \sum_{i=1}^{m-1} h_i, \quad l = 1, 2, \ldots, h_m, m = 1, 2, \ldots, M-1. \tag{2}$$

Accordingly, the element positions of subarray 1, 2, . . ., M are $\mathbf{p}_1 d = [p(1,1), \ldots, p(N,1)]^T d$, $\mathbf{p}_2 d = [p(1,2), \ldots, p(N,2)]^T d$, . . ., and $\mathbf{p}_M d = [p(1,M), \ldots, p(N,M)]^T d$, respectively. The element positions of M-1 virtual subarrays are $\mathbf{q}_1 d = [q(1,1), \ldots, q(h_1,1)]^T d$, $\mathbf{q}_2 d = [q(1,2), \ldots, q(h_2,2)]^T d$, . . ., and $\mathbf{q}_{M-1} d = [q(1, M-1), \ldots, q(h_{M-1}, M-1)]^T d$, respectively.

Therefore, all of the sensors can form a virtual contiguous ULA with $Z = MN + \sum_{i=1}^{m-1} h_i$ elements. Assume that the array receives S + 1 narrowband signals from far-field signal sources. The desired signal impinges upon the DDSA from direction θ_0, and S interfering signals come from the directions $\theta_1, \theta_2, \ldots, \theta_S$, respectively. The DDSA observation vector $\mathbf{x}(k) \in C^{MN \times 1}$ at time k can be modeled as

$$\mathbf{x}(k) = \mathbf{x}_d(k) + \sum_{i=1}^{S} \mathbf{x}_i(k) + \mathbf{n}(k), \tag{3}$$

where $\mathbf{x}_d(k)$, $\mathbf{x}_i(k)$, and $\mathbf{n}(k)$ are the desired signal, interference, and noise, respectively, which are statistically independent of each other. The element of the noise vector $\mathbf{n}(k)$ is assumed to be independent and identically distributed complex Gaussian variables with zero mean and variance δ_n^2.

The beamforming output at time k can be expressed as

$$y(k) = \mathbf{w}^H \mathbf{x}(k), \tag{4}$$

where $\mathbf{w} = [w_0, w_1, \ldots, w_{MN-1}]^T$ denotes the weight vector of the beamformer and $(\cdot)^{\mathrm{H}}$ denotes the Hermitian transpose operation. The output SINR can be obtained from

$$\mathrm{SINR} = \frac{\delta_d^2 \left| \mathbf{w}^H \mathbf{a}(\theta_0) \right|^2}{\mathbf{w}^H \mathbf{R}_{i+n} \mathbf{w}}, \tag{5}$$

where δ_d^2 denotes the power of the desired signal, $\mathbf{a}(\theta_0) = [\mathbf{a}_1^T(\theta_0), \mathbf{a}_2^T(\theta_0), \ldots, \mathbf{a}_M^T(\theta_0)]^T \in C^{MN \times 1}$ denotes the steering

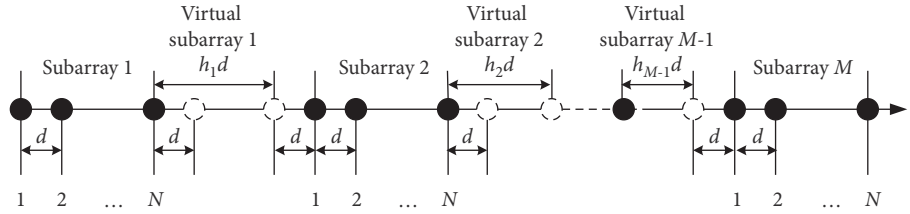

Figure 1: Geometry structure of DDSA.

vector corresponding to the direction θ_0, $\mathbf{a}_m(\theta_0) = [\exp(-j\mu p(1, m)d \sin \theta_0), \exp(-j\mu p(2, m)d \sin \theta_0), \ldots, \exp(-j\mu p(N, m)d \sin \theta_0)]^T \in C^{N\times 1}$, $\mu = ((2\pi)/\lambda)$, λ denotes the carrier wavelength, and $\mathbf{R}_{i+n} \in C^{MN\times MN}$ denotes the theoretical INCM, which can be reconstructed by

$$\mathbf{R}_{i+n} = \sum_{i=1}^{S} \delta_i^2 \mathbf{a}(\theta_i)\mathbf{a}^H(\theta_i) + \delta_n^2 \mathbf{I}_{MN}, \tag{6}$$

where δ_i^2 denotes the power of the i-th interfering signal and $\mathbf{I}_{MN}$ stands for an $MN \times MN$ identity matrix. By maximizing the output SINR (5), the optimal weight vector can be expressed as

$$\mathbf{w}_{\text{opt}} = \frac{\mathbf{R}_{i+n}^{-1}\mathbf{a}(\theta_0)}{\mathbf{a}^H(\theta_0)\mathbf{R}_{i+n}^{-1}\mathbf{a}(\theta_0)} \in C^{MN\times 1}, \tag{7}$$

which is a function of the interference energy δ_i^2, noise power δ_n^2, and the DOAs $\theta_s(s = 0, 1, \ldots, S)$ of the desired signal and interferers. From (7), the $MN \times 1$ weight vector $\mathbf{w}_{\text{opt}}$ can be obtained, which corresponds to MN physical elements of the DDSA. However, the sparse distribution of M subarrays may result in the grating lobes and high sidelobe levels. Therefore, to suppress grating lobes and high sidelobes, it is a practical way to reconstruct the received signals of $H = \sum_{i=1}^{M-1} h_i$ virtual elements and form a virtual contiguous ULA. By reconstructing the INCM of the virtual ULA, the adaptive beamforming is used for suppressing the interfering signals. To make the desired signal keep phase congruency among multiple channels, only the interfering signals received by the virtual elements are reconstructed. In addition, it is difficult to accurately estimate the DOA of the desired signal at low SNR, which may result in the drift of beam direction.

3. Proposed Algorithm

In this section, a robust adaptive beamforming algorithm using virtual array elements is proposed. Based on the DOA estimation of the desired signal and interferers, the received data on the virtual elements and the INCM of the virtual contiguous array can be reconstructed. Introducing the virtual array elements can greatly increase the DOF of the proposed beamformer and improve the anti-interference performance. With the INCM of the virtual ULA and the steering vector of the desired signal, the weight vector can be obtained, which must be used for processing the rearranged data set received by the actual and virtual elements.

3.1. DOA Estimation of the DDSA. As shown in Figure 2, the DDSA is divided into two subarray sets A_{z1} and A_{z2}. The subarray set A_{z1} consists of the first $N-1$ sensors of each actual subarray, and the subarray set A_{z2} is composed of the last $N-1$ elements of each actual subarray. Between A_{z1} and A_{z2}, there is a space-translation invariant $d = (\lambda/2)$. Therefore, the ESPRIT algorithm can be used for DOA estimation, and there is no ambiguity in the DOA estimation results.

If the DDSA observation vector at time k can be expressed as $\mathbf{x}(k) \in C^{MN\times 1}$, the received data of the subarray sets A_{z1} and A_{z2} can be, respectively, written as

$$\begin{aligned} \mathbf{x}_{z1}(k) &= \mathbf{J}_{z1}\mathbf{x}(k), \\ \mathbf{x}_{z2}(k) &= \mathbf{J}_{z2}\mathbf{x}(k), \end{aligned} \tag{8}$$

where $\mathbf{J}_{z1} = \mathbf{I}_M \otimes [\mathbf{I}_{N-1}; 0_{(N-1)\times 1}]$, $\mathbf{J}_{z2} = \mathbf{I}_M \otimes [0_{(N-1)\times 1}; \mathbf{I}_{N-1}]$, $\mathbf{I}$ denotes the identity matrix, and $0_{(N-1)\times 1}$ denotes the $(N-1)\times 1$ vector of all zeros. Assume that the interfering signals are much stronger than noise, and we can neglect the effect of noise in (8). For the s-th interfering signal, the rotation-invariant relationship can be expressed as

$$e^{-j\mu d \sin\theta_s}\mathbf{J}_{z1}\mathbf{a}(\theta_s) = \mathbf{J}_{z2}\mathbf{a}(\theta_s), \tag{9}$$

where θ_s denotes the DOA of the s-th interferer. Consider that there are $\widetilde{S}$ incident signals received by the DDSA, and the DOAs are $\theta_1, \ldots, \theta_{\widetilde{S}}$, respectively. Then, the rotation-invariant relationship can be further written as

$$\mathbf{J}_{z1}\mathbf{A}\Gamma = \mathbf{J}_{z2}\mathbf{A}, \tag{10}$$

where $\Gamma = \text{diag}([e^{-j\mu d \sin\theta_1}, \ldots, e^{-j\mu d \sin\theta_{\widetilde{S}}}])$ and $\mathbf{A} = [\mathbf{a}(\theta_1), \ldots, \mathbf{a}(\theta_{\widetilde{S}})]$ denotes the array manifold of the DDSA. Because both the subspace spanned by the steering vectors and the signal subspace belong to the same subspace, there is an invertible matrix Φ, satisfying

$$\mathbf{U}_s = \mathbf{A}\Phi, \tag{11}$$

where $\mathbf{U}_s$ denotes the signal subspace. In practice, $\mathbf{U}_s$ can be estimated by performing eigendecomposition of the sample covariance matrix, and the number of the incident signals $\widetilde{S}$ can be correctly estimated by the methods in [18, 19]. From (11), equation (10) can be updated to

$$\mathbf{E}_{z1}\Psi = \mathbf{E}_{z2}, \tag{12}$$

where $\mathbf{E}_{z1} = \mathbf{J}_{z1}\mathbf{U}_s$, $\mathbf{E}_{z2} = \mathbf{J}_{z2}\mathbf{U}_s$, and $\Psi = \Phi^{-1}\Gamma\Phi$. Therefore, we can obtain the rotation-invariant relation matrix:

$$\widetilde{\boldsymbol{\Psi}} = \left(\mathbf{E}_{z1}^{H}\mathbf{E}_{z1}\right)^{-1}\mathbf{E}_{z1}^{H}\mathbf{E}_{z2}. \tag{13}$$

By performing eigendecomposition of matrix $\widetilde{\Psi}$, the DOA estimation can be obtained by

$$\widetilde{\theta}_s = -\arcsin\left\{\frac{\text{angle}(\rho_s)}{\mu d}\right\}, \quad 1 \le s \le \widetilde{S}, \tag{14}$$

where ρ_s denotes the s-th eigenvalue of the rotation-invariant relation matrix $\widetilde{\Psi}$. With the ESPRIT-like method [20, 21], the DOAs of the interfering signals can be accurately estimated, and it is the same to the desired signal at high SNR.

3.2. Data Reconstruction of the Virtual Contiguous Array. In general, the desired signal energy has a very large range of variation, and the input SNR can vary from −30 dB to +50 dB in the simulations. Due to the impact of DOA estimation errors, it is impossible to accurately estimate the phases and amplitudes of the desired signal, which can bring about bad impacts on the later data processing. However, the reconstruction errors of the interfering signals have different effects, which only change the positions and depths of the nulls. Moreover, the interference energy is usually much stronger than noise, which is helpful to improve the accuracy of DOA estimation. Through the virtual expansion, the DOF of the proposed beamformer is dramatically increased, and the nulls in the beampattern can be significantly deepened. Therefore, the interference reconstruction on the virtual elements can enhance the anti-interference capability of the proposed beamformer.

Owing to the narrowband assumption, there are only phase differences among the received signals on different array elements. For the m-th virtual subarray, the received interfering signals at the elements can be expressed as

$$\begin{aligned}
\breve{x}_i(1,m) &= \sum_{i=1}^{S} v_i \exp(j\phi_i)\exp\left(-j\mu q(1,m) d \sin\theta_i\right) \\
&= \sum_{i=1}^{S} a_i b_i^{q(1,m)}, \\
\breve{x}_i(2,m) &= \sum_{i=1}^{S} v_i \exp(j\phi_i)\exp\left(-j\mu q(2,m) d \sin\theta_i\right) \\
&= \sum_{i=1}^{S} a_i b_i^{q(2,m)}, \\
&\vdots \\
\breve{x}_i(h_m,m) &= \sum_{i=1}^{S} v_i \exp(j\phi_i)\exp\left(-j\mu q(h_m,m) d \sin\theta_i\right) \\
&= \sum_{i=1}^{S} a_i b_i^{q(h_m,m)},
\end{aligned} \tag{15}$$

where $a_i = v_i \exp(j\phi_i)$, $b_i = \exp(-j\mu d \sin\theta_i)$, and $v_i \exp(j\phi_i)$ denotes the i-th interfering signal. Casting the above equations in matrix form can get

$$\breve{x}_{i,m} = \mathbf{B}_{i,m}(\mathbf{q}_m)\mathbf{r}_i, \tag{16}$$

where

$$\begin{aligned}
\mathbf{B}_{i,m}(\mathbf{q}_m) &= \begin{pmatrix} b_1^{q(1,m)} & \cdots & b_S^{q(1,m)} \\ \vdots & \ddots & \vdots \\ b_1^{q(h_m,m)} & \cdots & b_S^{q(h_m,m)} \end{pmatrix}_{h_m \times S}, \\
\mathbf{r}_i &= \begin{pmatrix} a_1 \\ \vdots \\ a_S \end{pmatrix}_{S\times 1}, \\
\breve{x}_{i,m} &= \begin{pmatrix} \breve{x}(1,m) \\ \vdots \\ \breve{x}(h_m,m) \end{pmatrix}_{h_m \times 1}.
\end{aligned} \tag{17}$$

To reconstruct the received interfering signals on the virtual subarrays, the DOAs, magnitudes, and phases are needed. Assume that all interference energy is much stronger than noise, and then the DOAs of the interfering signals can be accurately estimated by the ESPRIT-like method in the last subsection. The angular sector Θ in which the desired signal is located can be obtained in advance, and the DOA estimation result can be written as $\widetilde{\theta} = [\widetilde{\theta}_0, \widetilde{\theta}_1, \ldots, \widetilde{\theta}_S]^{\mathrm{T}}$. On the actual subarray m, the energy of the interfering signals is much stronger than that of noise, and then the received data can be represented as

$$\mathbf{x}_m \doteq \mathbf{C}_m(\mathbf{p}_m)\mathbf{r}, \tag{18}$$

where

$$\begin{aligned}
\mathbf{C}_m(\mathbf{p}_m) &= (\mathbf{b}_0 \ \ \mathbf{B}_{i,m}(\mathbf{p}_m)) = \begin{pmatrix} b_0^{p(1,m)} & b_1^{p(1,m)} & \cdots & b_S^{p(1,m)} \\ \vdots & \vdots & \ddots & \vdots \\ b_0^{p(N,m)} & b_1^{p(N,m)} & \cdots & b_S^{p(N,m)} \end{pmatrix}_{N\times(S+1)}, \\
\mathbf{x}_m &= \begin{pmatrix} x(1,m) \\ \vdots \\ x(N,m) \end{pmatrix}_{N\times 1}, \\
\mathbf{r} &= \begin{pmatrix} a_0 \\ \mathbf{r}_i \end{pmatrix} = \begin{pmatrix} a_0 \\ a_1 \\ \vdots \\ a_S \end{pmatrix}_{(S+1)\times 1}.
\end{aligned} \tag{19}$$

Therefore, the signal vector $\mathbf{r}$ can be calculated by [16]

$$\widetilde{\mathbf{r}} = \left(\widetilde{\mathbf{C}}_m^{H}(\mathbf{p}_m)\widetilde{\mathbf{C}}_m(\mathbf{p}_m)\right)^{-1}\widetilde{\mathbf{C}}_m^{H}(\mathbf{p}_m)\mathbf{x}_m, \tag{20}$$

where $\widetilde{\mathbf{r}}$ is the estimation of the signal vector $\mathbf{r}$ in (18) and $\widetilde{\mathbf{C}}_m(\mathbf{p}_m)$ is the approximate matrix of $\mathbf{C}_m(\mathbf{p}_m)$ by the DOA estimate $\widetilde{\theta}_s$, $0 \le s \le S$. After that, the interfering signal vector $\mathbf{r}_i$ can be extracted by

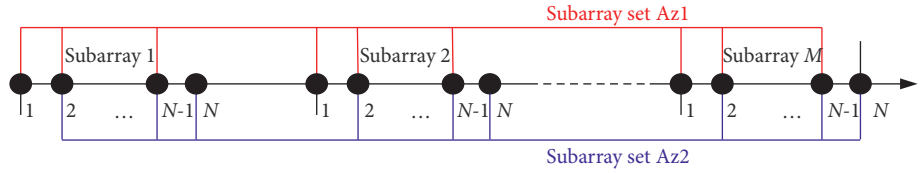

Figure 2: Subarray partition for DOA estimation.

$$\tilde{\mathbf{r}}_i = \tilde{\mathbf{r}}(2{:}\ S+1). \tag{21}$$

In the data processing, the mean values of the estimation $\tilde{\mathbf{r}}$ using multiple actual subarrays independently are adopted to cancel the effect of noise and improve the reconstruction accuracy. From (16), (18), and (20), the received data on the m-th virtual subarray can be constructed by

$$\tilde{\mathbf{x}}_m = \tilde{\mathbf{C}}_m(\mathbf{q}_m)\tilde{\mathbf{r}} = (\tilde{\mathbf{b}}_0(\mathbf{q}_m), \tilde{\mathbf{B}}_{i,m}(\mathbf{q}_m))\begin{pmatrix} \tilde{a}_0 \\ \tilde{\mathbf{r}}_i \end{pmatrix}, \tag{22}$$

where $\tilde{\mathbf{b}}_0(\mathbf{q}_m) = \exp(-j\mu\mathbf{q}_m d\sin\tilde{\theta}_0)$, $\tilde{\mathbf{B}}_{i,m}(\mathbf{q}_m) = \begin{pmatrix} \tilde{b}_1^q(1,m) & \cdots & \tilde{b}_S^q(1,m) \\ \vdots & \ddots & \vdots \\ \tilde{b}_1^q(h_m,m) & \cdots & \tilde{b}_S^q(h_m,m) \end{pmatrix}_{h_m\times S}$, and $\tilde{b}_i = \exp(-j\mu d\sin\tilde{\theta}_i), 1 \le i \le S$. Then, the received interfering signals $\tilde{\mathbf{x}}_{i,m}$ on the m-th virtual subarray can be constructed by $\tilde{\mathbf{x}}_{i,m} = \tilde{\mathbf{B}}_{i,m}(\mathbf{q}_m)\tilde{\mathbf{r}}_i$. By continuously processing multiple snapshots, the received data matrix $\tilde{\mathbf{X}}_m$ and interference data matrix $\tilde{\mathbf{X}}_{i,m}$ on the m-th virtual subarray can be obtained. Therefore, two new data matrices of the virtual contiguous array can be, respectively, constructed as

$$\hat{\mathbf{X}} = \left[\mathbf{X}_1; \tilde{\mathbf{X}}_1; \mathbf{X}_2; \tilde{\mathbf{X}}_2; \ldots; \mathbf{X}_{M-1}; \tilde{\mathbf{X}}_{M-1}; \mathbf{X}_M\right]_{Z\times N_c}, \tag{23}$$

$$\hat{\mathbf{X}}_p = \left[\mathbf{X}_1; \tilde{\mathbf{X}}_{i,1}; \mathbf{X}_2; \tilde{\mathbf{X}}_{i,2}; \ldots; \mathbf{X}_{M-1}; \tilde{\mathbf{X}}_{i,M-1}; \mathbf{X}_M\right]_{Z\times N_c}, \tag{24}$$

where $\hat{\mathbf{X}}$ is used for the power estimation of signal sources and $\hat{\mathbf{X}}_p$ is applied to the beamforming output with the weight vector.

3.3. DOA Estimation of the Desired Signal at Low SNR. If the input SNR of the desired signal is much greater than 0 dB, the DOA can be simultaneously estimated while processing the interfering signals, but the performance may decrease at low SNR. To solve this problem, we propose a novel DOA estimation method based on subarray adaptive beamforming. Using the m-th actual subarray, the first element is considered as the reference one. With the Capon spatial spectrum estimator, the INCM of the subarray m can be reconstructed by [22]

$$\tilde{\mathbf{R}}_{i+n,m} = \int_{\overline{\Theta}} \frac{\mathbf{a}_m(\theta)\mathbf{a}_m^H(\theta)}{\mathbf{a}_m^H(\theta)\mathbf{R}_m^{-1}\mathbf{a}_m(\theta)}\,d\theta, \tag{25}$$

where $\mathbf{R}_m = (1/N_c)\mathbf{X}_m\mathbf{X}_m^H$ is the sample covariance matrix of the subarray m, $\mathbf{a}_m(\theta) = [1, \exp(-j\mu d\sin\theta), \ldots, \exp(-j\mu(N-1)d\sin\theta)]^T$ is the steering vector, and $\overline{\Theta}$ is the complement sector of Θ, which is the angular sector in which the desired signal is located. In order to improve the beam pointing accuracy, the signal-plus-noise covariance matrix of the subarray m can be reconstructed by [23]

$$\tilde{\mathbf{R}}_{s+n,m} = \int_{\Theta} \frac{\mathbf{a}_m(\theta)\mathbf{a}_m^H(\theta)}{\mathbf{a}_m^H(\theta)\mathbf{R}_m^{-1}\mathbf{a}_m(\theta)}\,d\theta + \tilde{\delta}_n^2\mathbf{I}_N, \tag{26}$$

where $\tilde{\delta}_n^2$ is the noise power estimate, which can be replaced by the minimum eigenvalue of the sample covariance matrix $\mathbf{R}_m$. To estimate the actual steering vector $\tilde{\mathbf{a}}$, we can establish the optimization problem as follows [23]:

$$\begin{aligned} &\min_{\tilde{\mathbf{a}}} \tilde{\mathbf{a}}^H\tilde{\mathbf{R}}_{i+n,m}^{-1}\tilde{\mathbf{a}} \\ &\text{subject to} \quad \mathbf{a}_m^H(\theta_0')(\tilde{\mathbf{a}} - \mathbf{a}_m(\theta_0')) = 0, \\ &\tilde{\mathbf{a}}^H\tilde{\mathbf{R}}_{s+n,m}^{-1}\tilde{\mathbf{a}} \le \mathbf{a}_m^H(\theta_0')\tilde{\mathbf{R}}_{s+n,m}^{-1}\mathbf{a}_m(\theta_0'), \end{aligned} \tag{27}$$

where θ_0' is the presumed DOA of the desired signal. The optimization problem is a quadratically constrained quadratic programming problem, which can be solved by the convex optimization software, e.g., CVX [24]. Taking out the first and second items, we can get

$$\exp\left(-j\mu d\sin\tilde{\theta}_0\right) = a_1 = \frac{\tilde{\mathbf{a}}(2)}{\tilde{\mathbf{a}}(1)}. \tag{28}$$

Hence, the DOA of the desired signal can be estimated by

$$\begin{aligned} \tilde{\theta}_0 &= -\arcsin(\gamma(\mu d)), \\ \gamma &= \arctan\left(\frac{\text{imag}(a_1)}{\text{real}(a_1)}\right), \end{aligned} \tag{29}$$

where real$(\cdot)$ and imag$(\cdot)$, respectively, denote the real part and imaginary part of a complex number.

3.4. Adaptive Beamforming Using Virtual Array Elements. From (23), if the received data of the virtual contiguous array have been reconstructed, the covariance matrix can be calculated by

$$\hat{\mathbf{R}} = \frac{1}{N_c}\hat{\mathbf{X}}\hat{\mathbf{X}}^H \in C^{Z\times Z}. \tag{30}$$

To estimate the signal energy, we can formulate the convex optimization problem as follows [25, 26]:

$$\begin{aligned} &\min_{\mathbf{p}(\tilde{\boldsymbol{\theta}})} \left\|\hat{\mathbf{R}} - tGn\,q\text{diag}h(\mathbf{p}(\tilde{\boldsymbol{\theta}}))_{\mathbf{G}^H}\right\|_F^2 \\ &\text{subject to} \quad \mathbf{p}(\tilde{\boldsymbol{\theta}}) > 0, \end{aligned} \tag{31}$$

where $\|\cdot\|_F$ denotes the Frobenius norm, $\mathbf{p}(\tilde{\theta}) = [p(\tilde{\theta}_0), p(\tilde{\theta}_1), \ldots, p(\tilde{\theta}_S)]^T$ denotes the signal power vector with corresponding to the power estimate at the angle $\tilde{\theta}_s$, $\mathbf{G} = [\mathbf{a}_z(\tilde{\theta}_0), \mathbf{a}_z(\tilde{\theta}_1), \ldots, \mathbf{a}_z(\tilde{\theta}_S)]_{Z\times(S+1)}$ is the manifold

matrix of the whole array, and $\mathbf{a}_z(\tilde{\theta}_s) = [1, \exp(-j\mu d\sin(\tilde{\theta}_s)), \ldots, \exp(-j\mu(Z-1)\, d\sin(\tilde{\theta}_s))]^{\mathrm{T}} \in C^{Z\times 1}$. In practice, the covariance matrix $\hat{\mathbf{R}}$ is a positive semidefinite matrix; the inequality constraint in (31) can be neglected. Without the inequality constraint, the solution can be written as [25, 26]

$$\mathbf{p}(\tilde{\theta}) = \left(\mathbf{D}^H\mathbf{D}\right)^{-1}\mathbf{D}^H\hat{\mathbf{r}}, \tag{32}$$

where $\mathbf{D} = [\mathrm{vec}(\mathbf{a}_z(\tilde{\theta}_0)\mathbf{a}_z^{\mathrm{H}}(\tilde{\theta}_0)), \mathrm{vec}(\mathbf{a}_z(\tilde{\theta}_1)\mathbf{a}_z^{\mathrm{H}}(\tilde{\theta}_1)), \ldots, \mathrm{vec}(\mathbf{a}_z(\tilde{\theta}_S)\mathbf{a}_z^{\mathrm{H}}(\tilde{\theta}_S))]_{Z^2\times(S+1)}$, $\mathbf{r} = \mathrm{vec}(\hat{\mathbf{R}})_{Z^2\times 1}$, and $\mathrm{vec}(\cdot)$ denotes the vectorization operator. Consequently, the INCM of the virtual contiguous array can be reconstructed by

$$\tilde{\mathbf{R}}_{i+n} = \sum_{i=1}^{S} p\left(\tilde{\theta}_i\right)\mathbf{a}_z\left(\tilde{\theta}_i\right)\mathbf{a}_z^H\left(\tilde{\theta}_i\right) + \tilde{\delta}_n^2\mathbf{I}_Z. \tag{33}$$

With the steering vector $\mathbf{a}_z(\tilde{\theta}_0) = [1, \exp(-j\mu d\sin\tilde{\theta}_0), \ldots, \exp(-j\mu(Z-1)\, d\sin\tilde{\theta}_0)]^T$ corresponding to the estimated DOA $\tilde{\theta}_0$ of the desired signal, the weight vector of the proposed beamformer can be written as

$$\mathbf{w}_{\mathrm{pro}} = \frac{\tilde{\mathbf{R}}_{i+n}^{-1}\mathbf{a}_z\left(\tilde{\theta}_0\right)}{\mathbf{a}_z^H\left(\tilde{\theta}_0\right)\tilde{\mathbf{R}}_{i+n}^{-1}\mathbf{a}_z\left(\tilde{\theta}_0\right)}. \tag{34}$$

Therefore, the output data vector of the proposed beamformer can be obtained by

$$\hat{\mathbf{y}} = \mathbf{w}_{\mathrm{pro}}^H\hat{\mathbf{X}}_p. \tag{35}$$

For clarity, the flowchart of the proposed algorithm is shown in Figure 3, and the arithmetic steps can be summarized as follows:

(1) Estimate the DOAs $\tilde{\theta} = [\tilde{\theta}_0, \tilde{\theta}_1, \ldots, \tilde{\theta}_S]$ of the desired signal and interferers

(2) Calculate the approximate matrices $\tilde{\mathbf{C}}_m(\mathbf{p}_m)$ and $\tilde{\mathbf{C}}_m(\mathbf{q}_m)$ via (18) with the DOA estimation $\tilde{\theta}$

(3) Substitute $\tilde{\mathbf{C}}_m(\mathbf{p}_m)$ into (20), and estimate the signal vector $\tilde{\mathbf{r}}$

(4) Substitute $\tilde{\mathbf{C}}_m(\mathbf{q}_m)$ and $\tilde{\mathbf{r}}$ into (22), and reconstruct the received data $\tilde{\mathbf{X}}_m$ of the m-th virtual subarray

(5) Reconstruct the virtual data matrices $\hat{\mathbf{X}}$ via (23) and $\hat{\mathbf{X}}_p$ via (24)

(6) Estimate the signal energy vector $\mathbf{p}(\tilde{\theta})$ using (32)

(7) Reconstruct the INCM $\tilde{\mathbf{R}}_{i+n}$ of the virtual contiguous array via (33)

(8) Calculate the weight vector $\mathbf{w}_{\mathrm{pro}}$ of the proposed algorithm using (34)

(9) Substitute $\mathbf{w}_{\mathrm{pro}}$ and $\hat{\mathbf{X}}_p$ into (35) to obtain the beamforming output

The main computational complexity of the proposed algorithm is the DOA estimation of the desired signal at low SNR and the power estimation. The former has the cost $O(N^2L)$, where L is the number of sampling points in the whole spatial domain, and the latter costs the complexity of $O((S+1)^2(NM+H)^2)$. Therefore, the computational complexity of the proposed algorithm is $O(\max\{(S+1)^2(NM+H)^2, N^2L\})$. The algorithmic complexity of REC-CMRSVE is $O(\max\{L_1(MN)^2, (MN)^{3.5}\})$, where L_1 is the number of sampling points in $\overline{\Theta}$. The RAB-WCPO beamformer has complexity of $O(MN)^{3.5}$ due to solving the optimization problem. The computational complexity of SMID-JAW is $O(M^3N^2L_1)$, which is mainly dominated by the M times INCM reconstruction. Therefore, the proposed beamformer has less computational complexity when the number of virtual elements is less than that of actual ones.

3.5. Discussion. So far, the DDSA has played an increasingly important role in radar, sonar, and communication systems. The research object of DDSA in this paper is the subarray antennas distributed in different parts of the same carrier, such as aircraft, vehicle, and ship. The DDSA has some desirable attributes: (1) DDSA can be applied to mainlobe interference suppression; (2) by forming a long baseline array, DDSA can achieve very accurate angular locations of targets; (3) with the distributed arrangement of subarrays, the expanded antenna aperture can provide larger detection range; (4) for a given desired performance, the signal transmitting power can be reduced significantly [6, 27, 28]. However, the distributed subarrays may bring about some negative impacts on the beampattern. If the subarrays are uniformly sparse, this can result in grating lobes. If the subarrays are randomly arranged, this may bring about high sidelobes. From the view of application, the bad effects may lead to ambiguity in the actual positions of targets and to excess clutter background coming from grating lobes and high sidelobes [28]. To solve these problems, the gaps between subarrays are filled with virtual elements, and then a virtual contiguous array can be formed, which can effectively suppress grating lobes and high sidelobes. Moreover, the proposed method can also be used to deal with failure of some elements in uniform arrays. By reconstructing the received signals on the faulty elements, a virtual contiguous array can be rebuilt, which is helpful to improve the spatial resolution and interference rejection capability.

4. Simulation Results

In the simulations, consider that the DDSA contains two uniform linear subarrays with 8 elements spaced half a wavelength, and the gap between the subarrays is $h_1 = 16d$. Assume that the desired signal impinges upon the DDSA from the direction $\theta_0 = -10^\circ$, and three interfering signals come from the directions $\theta_1 = -40^\circ$, $\theta_2 = 30^\circ$, and $\theta_3 = 50^\circ$, respectively. The interference-to-noise ratio (INR) is set to 30 dB. The additive noise is presumed to be a complex circularly symmetric Gaussian zero-mean spatially and temporally white process. The number of snapshots is set to $N_c = 60$ while comparing the output SINR versus the input SNR, and the input SNR is fixed at 10 dB in the performance

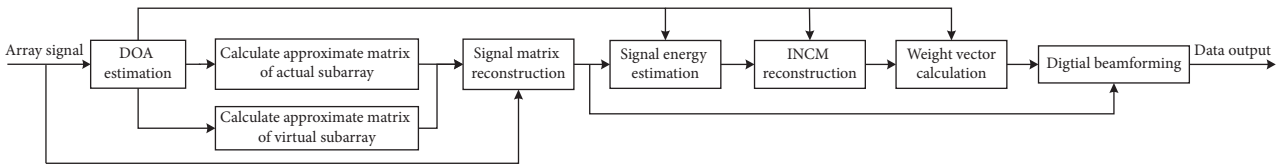

Figure 3: Flowchart of the proposed algorithm.

comparison versus the number of snapshots. Note that the random DOAs of the desired signal and the interferers change from trial to trial but remain fixed from snapshot to snapshot. For each scenario, the simulation results are provided as the average of 200 Monte Carlo trials.

The proposed adaptive beamformer is compared to the worst-case-based beamformer (RAB-WCPO) [29], distributed LCMV beamforming (DA-LCMV) [17], INCM reconstruction-based beamformer (REC-CMRSVE) [25], and the joint adaptive beamforming (SMIS-JAW) [6]. In addition, the optimal output SINR of the subarray is shown in the simulations to clearly demonstrate the advantages of the proposed beamformer. According to the MVDR criterion, the optimal output SINR is calculated by (5). The parameter $\varepsilon = 0.3$ is used in the RAB-WCPO, and the angular sector of the desired signal is set to be $\Theta = [\theta_0 - 5^\circ, \theta_0 + 5^\circ]$ while suppressing the sidelobe interference. The sampling grid is uniform in Θ and $\overline{\Theta}$ with 0.1° increment between adjacent grid points.

In [30], the DOF was defined by a difference set, which is expressed as

$$D = \mathrm{SD} \cup \mathrm{CD}, \tag{36}$$

where SD and CD denote the self-difference set and cross-difference set of two integer number sets, respectively. Then, the DOF is equal to the total number of the distinct elements in the difference set D, and the virtual array aperture is quantified as

$$\mathrm{VAA} = \max\{D\} - \min\{D\}. \tag{37}$$

According to parameter settings for the simulations, the element positions of two uniform linear subarrays can be regarded as two integer number sets. According to [30], the self-difference set is $\mathrm{SD}_0 = \{-7, -6, -5, -4, -3, -2, -1, 0, 1, 2, 3, 4, 5, 6, 7\}$, and the cross-difference set is $\mathrm{CD}_0 = \{\pm (17, 18, 19, 20, 21, 22, 23, 24, 25, 26, 27, 28, 29, 30, 31)\}$. Hence, the difference set is $D_0 = \mathrm{SD}_0 \cup \mathrm{CD}_0 = \{0, \pm (1, 2, 3, 4, 5, 6, 7, 17, 18, 19, 20, 21, 22, 23, 24, 25, 26, 27, 28, 29, 30, 31)\}$, which contains 45 distinct elements. Consequently, the DOF of DDSA is 45, and the virtual array aperture is $\mathrm{VAA}_0 = 62d$. By the proposed scheme, a virtual uniform linear array can be formed, which is composed of 32 contiguous elements, including the actual elements and virtual elements. The difference set is $D_1 = \{0, \pm (1, 2, 3, 4, 5, 6, 7, 8, 9, 10, 11, 12, 13, 14, 15, 16, 17, 18, 19, 20, 21, 22, 23, 24, 25, 26, 27, 28, 29, 30, 31)\}$, and then the proposed scheme can change the DOF to 63. Due to $\max\{D_0\} = \max\{D_1\}$ and $\min\{D_0\} = \min\{D_1\}$, the virtual array aperture remains unchanged, i.e., $\mathrm{VAA}_1 = \mathrm{VAA}_0$. Because the positions of the first and last elements are not changed, the physical aperture of the tested DDSA remains the same. In the simulations, the proposed scheme increases the DOF from 45 to 63, and the array aperture remains unchanged.

4.1. Simulation for Beampattern. In the first example, the mainlobe width and sidelobe levels of the beampattern are examined. Assume that the DOAs of the desired signal and three interferers are accurately known. As the desired signal components in the sample covariance matrix may degrade the performance of some tested beamformers, the input SNR is set to be 0 dB. In the simulations, the DOA of the first interferer is changed from -40° to -6°, which can form the mainlobe jamming. Note that, in this scenario, the angular sector of the desired signal is set to be $\Theta = [-13^\circ, -7^\circ]$. Figures 4(a) and 4(b), respectively, correspond to beampattern with sidelobe and mainlobe interferences. It can be seen from Figure 4(a) that, as a result of employing more elements spaced half a wavelength, the mainlobe width and sidelobe levels of the proposed algorithm are better than those of the other tested beamformers while suppressing the sidelobe interference. Moreover, the proposed beamforming beampattern has deeper nulls with the normalized amplitudes below -120 dB. Figure 4(b) shows that the subarray mainlobe interference is effectively suppressed by the virtual contiguous array, while the other tested beamformers cannot resist the beam-pointing drift while suppressing the mainlobe jamming, including the optimal beamformer. From the beampatterns, the proposed beamformer possesses the obvious advantages in many aspects, such as mainlobe width, sidelobe levels, null depth, and beam direction.

4.2. Performance Comparison of Different Arrays. In the second example, the DDSA with the proposed algorithm is compared to the traditional ULA and nonuniform arrays, including coprime array and nested array. Assume that, for the arrays taken into the comparison, the DOA of the desired signal and INCM can be accurately obtained in advance, and then the optimal beamformer based on the minimum variance distortionless response (MVDR) criterion can be applied to the traditional ULA, coprime array, and nested array, respectively. Note that all the arrays involved in the experiments have 16 elements. The ULA is composed of 16 omnidirectional elements with interspacing d. The coprime array contains two subarrays, whose first element is shared. The first subarray has 8 elements with interelement spacing $9d$, while the second subarray has 9 elements with interelement spacing $8d$. The nested array is a concatenation of an inner ULA and an outer ULA, and both of them have 8 elements. The spacing between two adjacent elements of the inner ULA is half a wavelength d, and the intersensor

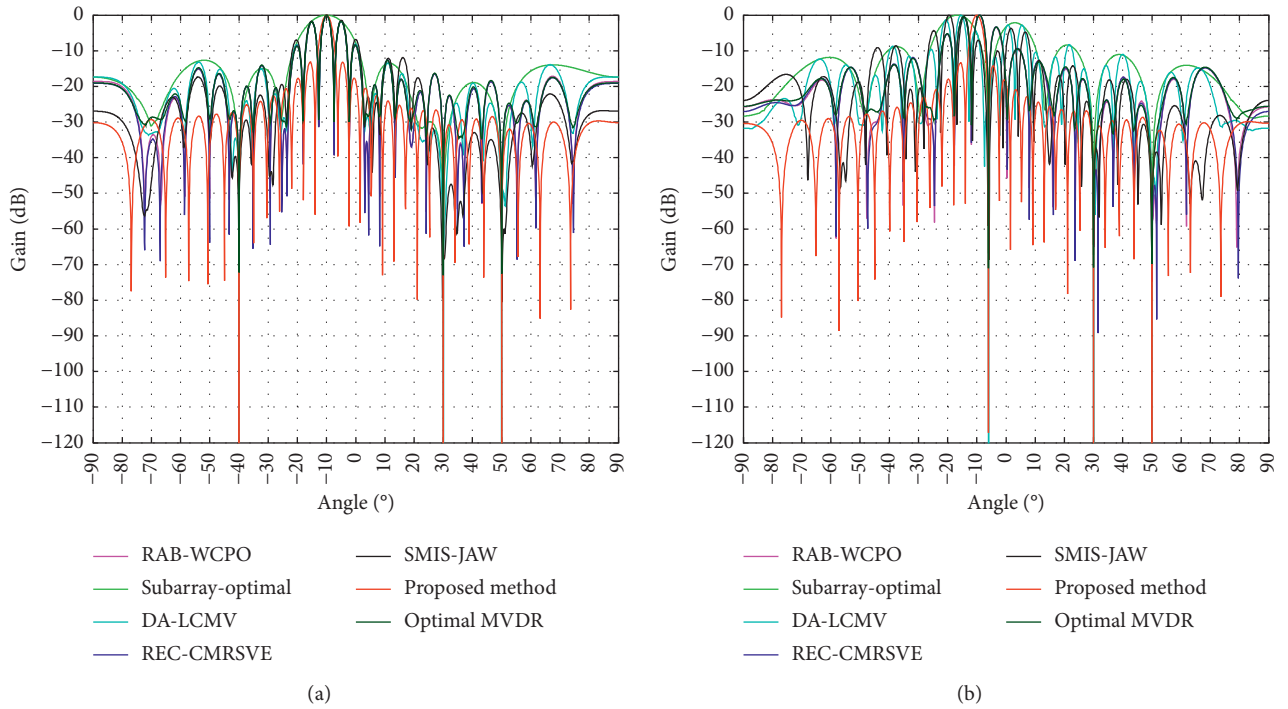

Figure 4: First example: (a) beampattern in the case of sidelobe interferences and (b) beampattern in the case of mainlobe and sidelobe interferences.

spacing of the outer ULA is $9d$. Assume that the desired signal comes from the direction $\theta_0 = 0^\circ$, and three interfering signals impinge upon the arrays from $\theta_1 = -40^\circ$, $\theta_2 = 30^\circ$, and $\theta_3 = 50^\circ$, respectively. In the case of sidelobe interferences, the beampattern is shown in Figure 5(a), and Figure 5(b) compares the output SINR versus input SNR with the number of snapshots $K = 200$. Figure 5(a) demonstrates that the mainlobe width of the proposed scheme is smaller than that of the ULA, and the sidelobe levels are much lower than those of the nonuniform arrays. As shown in Figure 5(b), the proposed scheme can achieve the best performance of the other tested arrays. When the DOA of the first interference changes from -40° to 4° and other DOAs remain unchanged, the interfering signal in the main lobe may have different impacts on the tested arrays. Note that, in this simulation, the angular sector of the desired signal is set to be $\Theta = [-3^\circ, +3^\circ]$. In the case of mainlobe and sidelobe interferences, Figure 5(c) gives the beampattern, and Figure 5(d) depicts the output SINR versus input SNR with the number of snapshots $K = 200$. It is shown in Figure 5(c) that the beam pointing of the ULA deviates from the preset direction, while other schemes maintain the correct direction. From Figure 5(d), it is indicated that while suppressing the mainlobe interference, the proposed scheme outperforms the other tested arrays with the optimal beamformer. Simulation results demonstrate that the proposed scheme can achieve or even exceed the optimal beamformers of the traditional ULA, coprime array, and nested array.

4.3. Adaptive Interference Rejection Capability. In the third example, the performance of adaptive interference rejection capability is examined. The DOA of the desired signal is exactly known, and the random DOA error of the interferers is uniformly distributed in $[-4^\circ, 4^\circ]$. That is to say, the DOAs of three interferers are uniformly distributed in $[-44^\circ, -36^\circ]$, $[26^\circ, 34^\circ]$, and $[46^\circ, 54^\circ]$, respectively. The output SINR performance versus the input SNR and the number of snapshots are shown in Figures 6(a) and 6(b), respectively. It is demonstrated from Figure 6(a) that if the DOA of the desired signal is known, DA-LCMV, REC-CMRSVE, and the proposed algorithm have similar performance and are superior to other tested beamformers. Figure 6(b) shows that both DA-LCMV and REC-CMRSVE need more snapshots to achieve good performance. The figures demonstrate that the proposed beamformer enjoys a better performance improvement in this scenario. Compared with the subarray optimal beamformer, the proposed beamformer through multiple subarray synthesis significantly outperforms that of single subarray.

4.4. Mainlobe Jamming of Subarray. In the fourth example, the impact of mainlobe jamming is considered. Assume that the DOAs of three interferers are -6°, -40°, and 50°, respectively. For each distributed subarray, the first interferer has located in the main lobe of subarray beamforming. In this scenario, all DOAs of the desired signal and interferers are unknown, and the angular set Θ of the

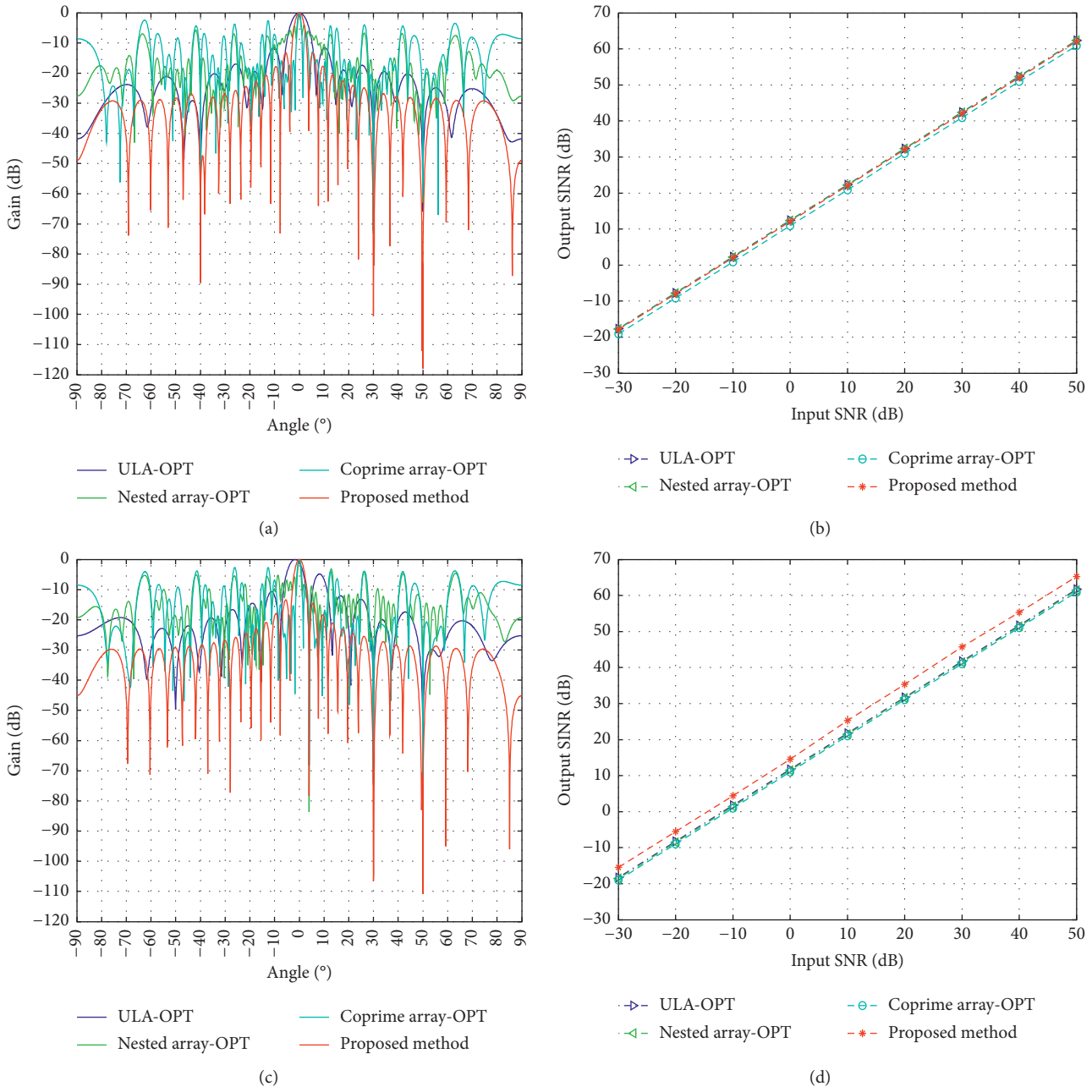

Figure 5: Second example: (a) beampattern in the case of sidelobe interferences, (b) output SINR versus input SNR while suppressing sidelobe interferences, (c) beampattern in the case of mainlobe and sidelobe interferences, and (d) output SINR versus input SNR while suppressing mainlobe and sidelobe interferences.

desired signal is set to be $[-13^\circ, -7^\circ]$. The DOA of the mainlobe jamming is fixed at -6°, and two sidelobe interferers are uniformly distributed in $[26^\circ, 34^\circ]$ and $[46^\circ, 54^\circ]$, respectively. While the number of snapshots is fixed at $N_c = 120$, the output SINR versus the input SNR is shown in Figure 7(a). When the input SNR is set as 10 dB, Figure 7(b) demonstrates the performance curves versus the number of snapshots. It can be seen from the figures that the proposed method dramatically outperforms other tested beamformers, even the optimal beamformer. That is because the beam-pointing drift while suppressing the mainlobe jamming, which has been verified in Figure 4(b), seriously degrades the performance of the optimal beamformer. Figure 7(b) shows that, with the increase of the number of snapshots, the performance of the proposed beamformer approaches or even exceeds the optimal beamformer when the number of snapshots is greater than 90. Therefore, the proposed algorithm significantly outperforms the other tested methods including the optimal beamformers in the case of mainlobe jamming.

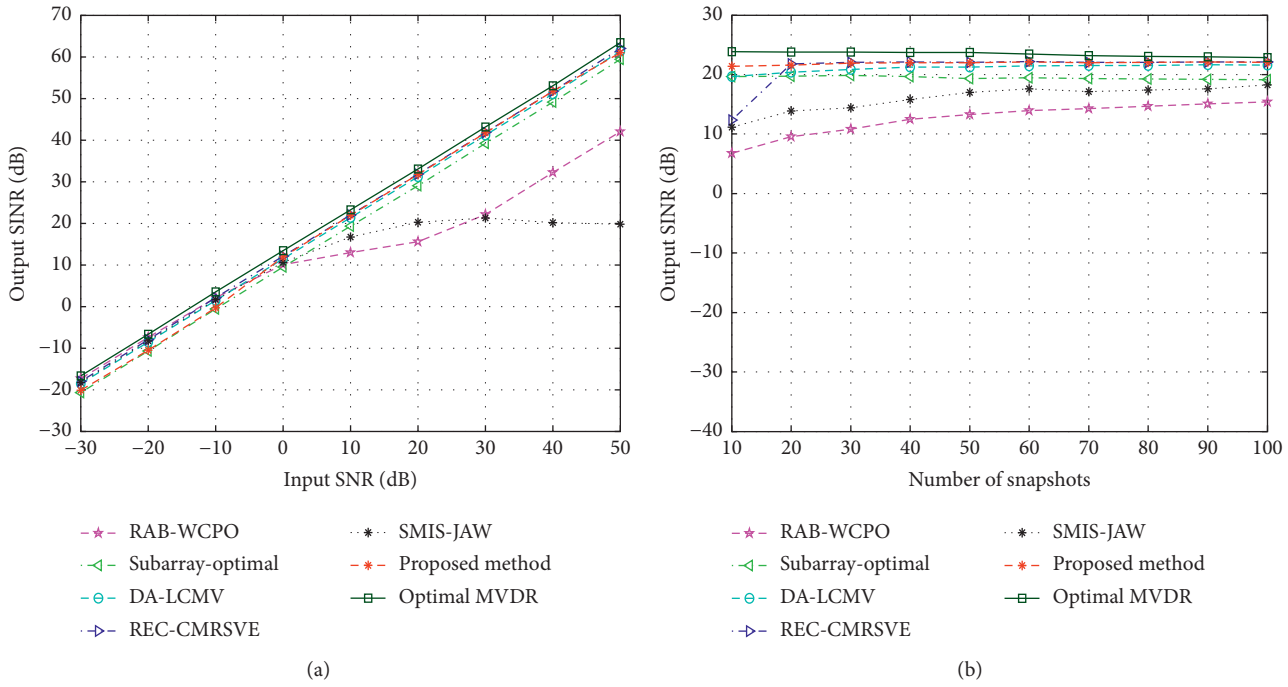

Figure 6: Third example: (a) output SINR versus input SNR and (b) output SINR versus number of snapshots.

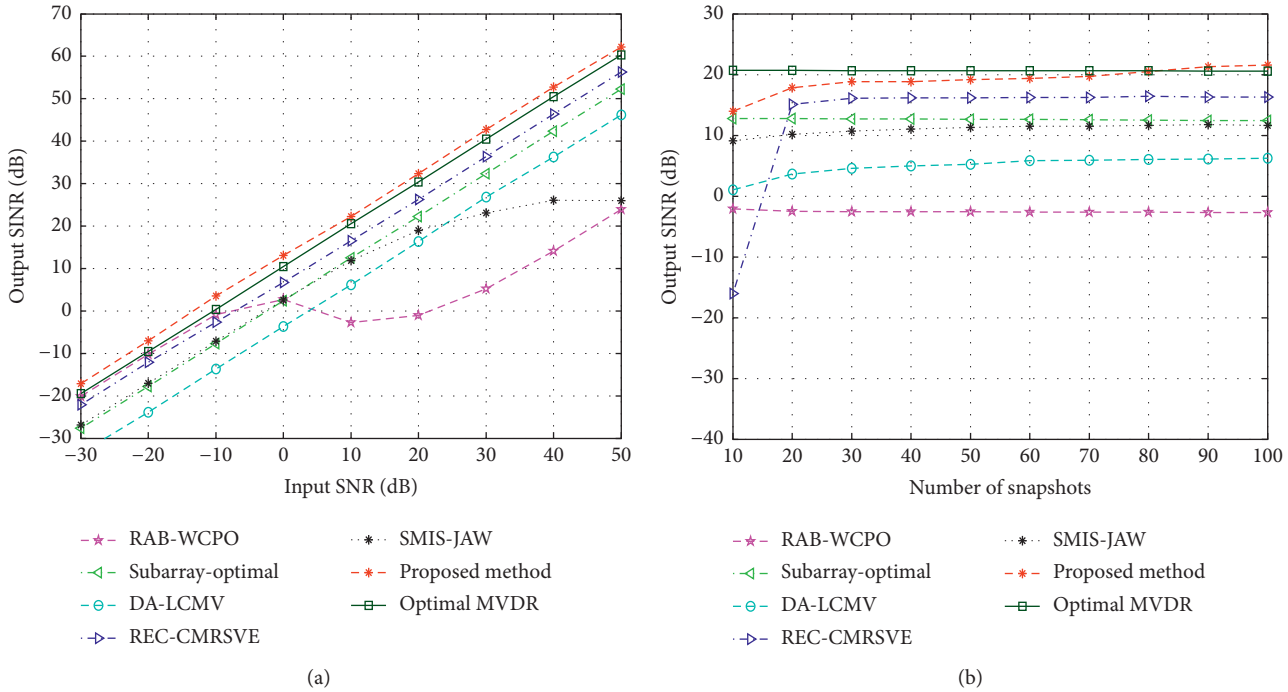

Figure 7: Fourth example: (a) output SINR versus input SNR and (b) output SINR versus number of snapshots.

4.5. Random Signal Look Direction Mismatch. In the fifth example, the influence of random signal direction errors is examined. The actual DOA of the desired signal is uniformly distributed in $[-13^\circ, -7^\circ]$, and the interference DOAs are uniformly distributed in $[-44^\circ, -36^\circ]$, $[26^\circ, 34^\circ]$, and $[46^\circ, 54^\circ]$, respectively. Figure 8(a) compares the output SINR versus the input SNR, and the output SINR against the number of snapshots is displayed by Figure 8(b). Figure 8(a) demonstrates that when the input SNR is greater than 0 dB, the proposed algorithm is very close to the optimal beamformer. Despite the DOA estimation errors at low SNRs make the performance of the proposed beamformer degrade slightly, whose output SINR is close to that of the subarray optimal beamformer, but the output SINR gradually approaches the optimal beamformer

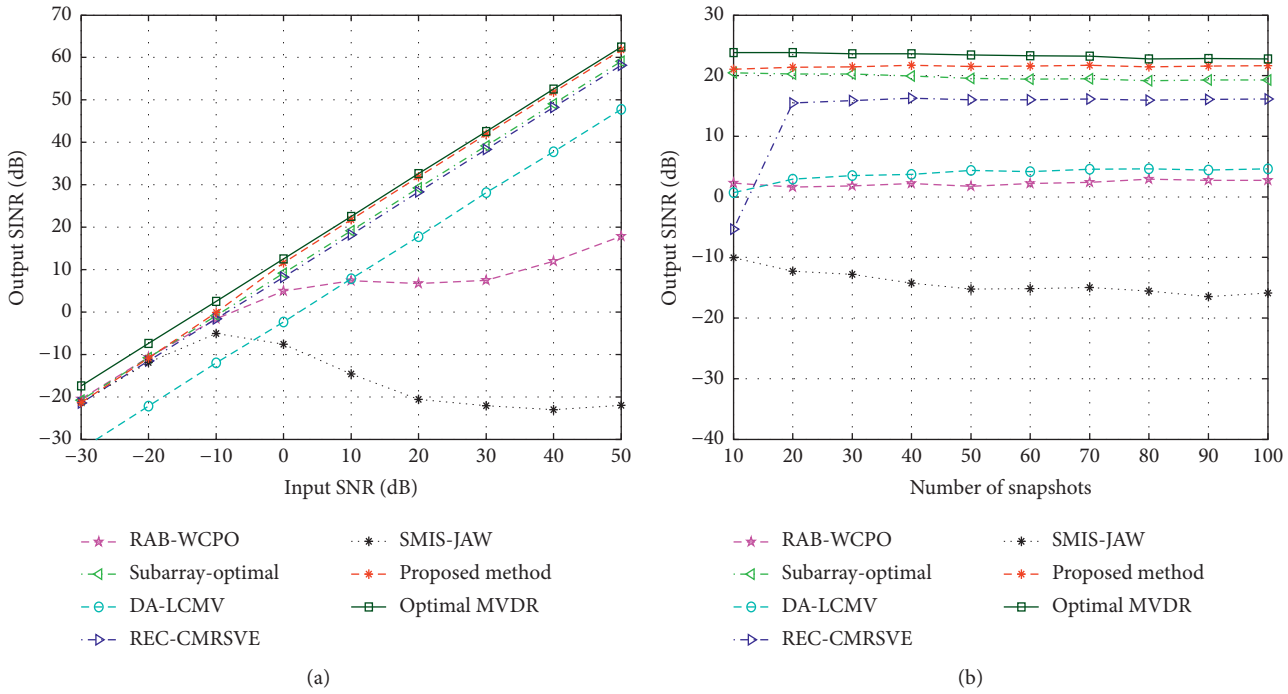

Figure 8: Fifth example: (a) output SINR versus input SNR and (b) output SINR versus number of snapshots.

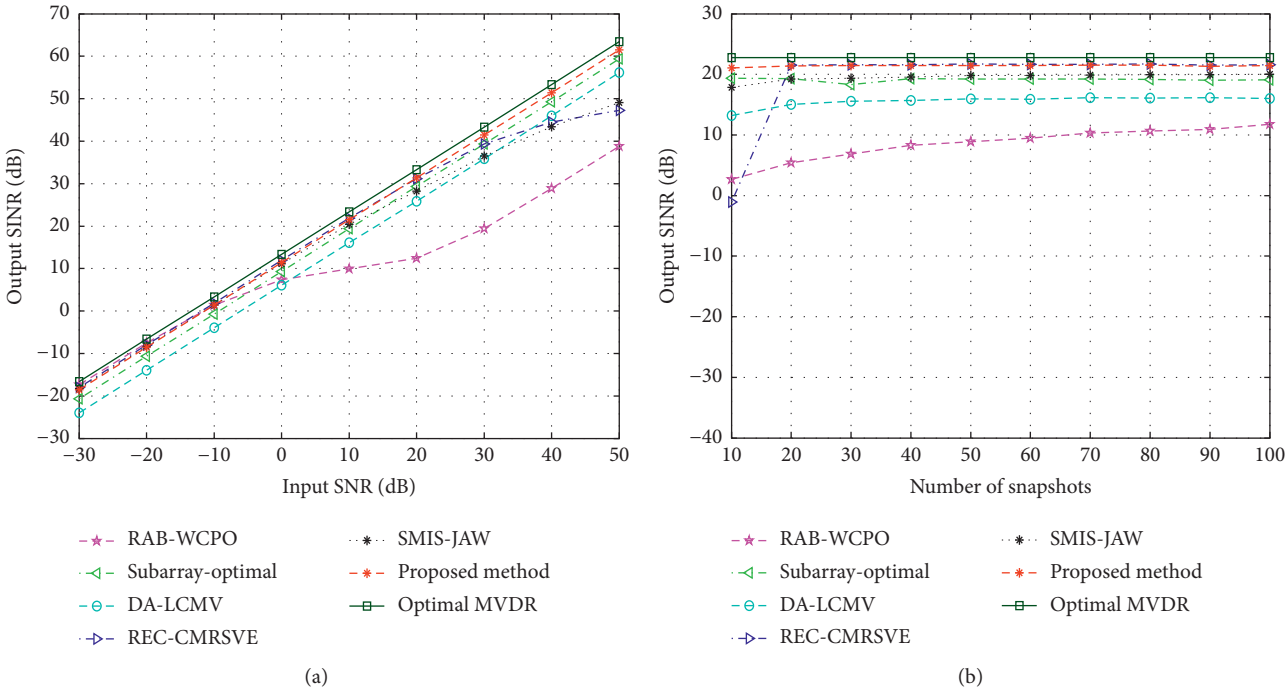

Figure 9: Sixth example: (a) output SINR versus input SNR and (b) output SINR versus number of snapshots.

when the input SNR is higher than −20 dB. It is seen from Figure 8(b) that, with the increase of the number of snapshots, the output SINR of the proposed beamformer is very close to the optimal beamformer, and the proposed algorithm outperforms the other tested beamformers.

4.6. Incoherent Local Scattering. In the last example, we consider the influence of incoherent local scattering on performance of the tested beamformers. Assume that the desired signal has a time-varying spatial signature as follows [23, 31]:

$$\mathbf{a}(k) = s_0(k)\mathbf{a}(\theta_0) + \sum_{l=1}^{4} s_l(k)\mathbf{a}(\theta_l), \tag{38}$$

where $s_p(k) \sim N(0,1)$, $p = 0,1,2,3,4$ are independently and identically distributed zero-mean complex Gaussian random variables changing from snapshot to snapshot; $\theta_l, l = 1,2,3,4$ are independently normally distributed in $N(\theta_0, 2^\circ)$. Note that θ_l changes both from trial to trial and from snapshot to snapshot. In this scenario, the signal covariance matrix $\mathbf{R}_s$ is no longer a rank-one matrix, and the optimal SINR should be obtained by [23, 28]

$$\mathrm{SINR}_{\mathrm{opt}} = \frac{\mathbf{w}_{\mathrm{opt}}^H \mathbf{R}_s \mathbf{w}_{\mathrm{opt}}}{\mathbf{w}_{\mathrm{opt}}^H \mathbf{R}_{i+n} \mathbf{w}_{\mathrm{opt}}}, \tag{39}$$

which is maximized by

$$\mathbf{w}_{\mathrm{opt}} = P\left\{\mathbf{R}_{i+n}^{-1}\mathbf{R}_s\right\}, \tag{40}$$

where $P\{\cdot\}$ denotes the principal eigenvector of a matrix. Figures 9(a) and 9(b) display the beamforming performance curves versus the input SNR and the number of snapshots, respectively. It can be seen from Figure 9(a) that when the input SNR is lower than 20 dB, both the proposed algorithm and REC-CMRSVE outperform the other tested methods, but the performance of REC-CMRSVE degrades with the further increase of input SNR. The output SINR of the proposed method has always been very close to that of the optimal beamformer. Figure 9(b) shows that, with the increase of the number of snapshots, the performance of the proposed algorithm approaches that of the optimal beamformer. There is only a little SINR loss for the proposed beamformer because the DOF has been greatly increased and the interfering signals can be effectively suppressed. Therefore, the proposed beamforming algorithm outperforms other tested beamformers in the case of incoherent local scattering.

5. Conclusion

In this paper, a novel robust adaptive beamforming algorithm for DDSA is proposed by virtual reconstruction. The gaps between the distributed subarrays are filled with the virtual elements, and then a new contiguous array can be formed. By dividing the DDSA into two rotation-invariant subarray sets, the DOAs can be accurately estimated by the ESPRIT-like method, and the received interfering signals on the virtual elements can be successfully reconstructed. At low SNRs, the steering vector of the desired signal can be obtained by solving the optimization problem. Based on the power estimation of the interfering signals, the INCM of the virtual contiguous array can be reconstructed, and then the weight vector of the proposed beamformer can be obtained. Without increasing the number of actual elements, the proposed algorithm greatly improves the DOF to enhance the interference rejection capability. Note that the weight vector must be applied to the rearranged data matrix received by the actual and virtual elements. With the virtual elements forming a contiguous array, the proposed beamforming algorithm can effectively suppress the grating lobes, reduce the mainlobe width, and degrade sidelobe levels. Simulation results highlight the validity and effectiveness of the proposed algorithm.

Data Availability

The data used to support the findings of this study are included within the article.

Conflicts of Interest

The authors declare no conflicts of interest.

Authors' Contributions

Jian Lu and Jian Yang contributed to conceptualization and methodology; Jian Lu and Bo Hou were responsible for software, validation, and investigation; Jian Lu and Bo Hou contributed to formal analysis; Jian Yang and Zhiyong Yu contributed to data curation; Jian Lu and Zhiyong Yu prepared the original draft; Jian Lu, Fengchao Zhu, and Guangbin Liu reviewed and edited the manuscript; Fengchao Zhu and Zhiyong Yu contributed to visualization; Guangbin Liu supervised the study; Jian Yang, Fengchao Zhu and Bo Hou contributed to project administration and funding acquisition.

Acknowledgments

This research was funded by the National Natural Science Foundation of China (62071481, 62071480, 62003363, and 61501471).

References

[1] Z. Li, C. Li, X. Chen, and W. Wang, "Beamforming in distributed antenna systems based on successive convex approximation and dual decomposition," in *Proceedings of the 11th International Conference on Wireless Communications and Signal Processing (WCSP)*, pp. 23–25, Xi'an, China, October 2019.

[2] B.-K. Feng and D. C. Jenn, "Two-way pattern grating lobe control for distributed digital subarray antennas," *IEEE Transactions on Antennas and Propagation*, vol. 63, no. 10, pp. 4375–4383, 2015.

[3] H. Zhang, J. Luo, X. Chen, Q. Liu, and T. Zeng, "Fresnel based frequency domain adaptive beamforming for large aperture distributed array radar," in *Proceedings of the 2016 IEEE International Conference on Signal Processing, Communications and Computing (ICSPCC)*, pp. 5–8, Hong Kong, China, August 2016.

[4] X. Chen, T. Shu, K.-B. Yu, J. He, and W. Yu, "Joint adaptive beamforming techniques for distributed array radars in multiple mainlobe and sidelobe jammings," *IEEE Antennas and Wireless Propagation Letters*, vol. 19, no. 2, pp. 248–252, 2020.

[5] S. Li, H. Zhang, X. Yang, Y. Sun, and Q. Liu, "Spatial multi-interference suppression based on joint adaptive weight for distributed array radar," in *Proceedings of the IEEE Radar Conference (RadarConf)*, pp. 22–26, Boston, MA, USA, April 2019.

[6] Y. Han, F. Zhou, X. Tian, and Y. Chen, "Distributed and parallel subarray beamforming for underwater real-time 3-D

acoustic imaging," in *Proceedings of the. 2012 2nd International Conference on Computer Science and Network Technology*, pp. 29–31, Changchun, China, December 2012.

[7] M. A. Maleki and M. Ahmadian, "Distributed robust beamforming in multi-user relay network," in *Proceedings of the 2014 IEEE Wireless Communications and Networking Conference (WCNC)*, pp. 6–9, Istanbul, Turkey, April 2014.

[8] Q. Pang, X. Wang, W. Wan, Y. Zhao, and X. Gu, "Coordinated beamforming for energy efficient transmission in distributed antenna systems," in *Proceedings of the 2015 IEEE 26th Annual International Symposium on Personal, Indoor, and Mobile Radio Communications (PIMRC)*, pp. 2–4, Hong Kong, China, September 2015.

[9] F. Quitin, A. T. Irish, and U. Madhow, "A scalable architecture for distributed receive beamforming: analysis and experimental demonstration," *IEEE Transactions on Wireless Communications*, vol. 15, no. 3, pp. 2039–2053, 2016.

[10] K. T. Wong and M. D. Zoltowski, "Direction-finding with sparse rectangular dual-size spatial invariance array," *IEEE Transactions on Aerospace and Electronic Systems*, vol. 34, no. 4, pp. 1320–1336, 1998.

[11] V. I. Vasylyshyn, "Unitary ESPRIT-based DOA estimation using sparse linear dual size spatial invariance array," in *Proceedings of the European Radar Conference (EURAD)*, pp. 3-4, Paris, France, October 2005.

[12] V. I. Vasylyshyn, "Direction of arrival estimation using ESPRIT with sparse arrays," in *Proceedings of the Sixth European Radar Conference (EuRAD)*, pp. 246–249, Paris, France, 2009.

[13] M. D. Zoltowski and K. T. Wong, "Closed-form eigenstructure-based direction finding using arbitrary but identical subarrays on a sparse uniform Cartesian array grid," *IEEE Transactions on Signal Processing*, vol. 48, no. 8, pp. 2205–2210, 2000.

[14] B.-K. Feng and D. C. Jenn, "Grating lobe suppression for distributed digital subarrays using virtual filling," *IEEE Antennas and Wireless Propagation Letters*, vol. 12, pp. 1323–1326, 2013.

[15] W. Chen, X. Xu, S. Wen, and Z. Cao, "Super-resolution direction finding with far-separated subarrays using virtual array elements," *IET Radar, Sonar & Navigation*, vol. 5, no. 8, pp. 824–834, 2011.

[16] D. Y. Levin, S. Markovich-Golan, and S. Gannot, "Distributed LCMV beamforming: considerations of spatial topology and local preprocessing," in *Proceedings of the IEEE Workshop on Applications of Signal Processing to Audio and Acoustics (WASPAA)*, pp. 15–18, New Paltz, NY, USA, October 2017.

[17] M. Wax and T. Kailath, "Detection of signals by information theoretic criteria," *IEEE Transactions on Acoustics, Speech, and Signal Processing*, vol. 33, no. 2, pp. 387–392, 1985.

[18] M. Wax and I. Ziskind, "Detection of the number of coherent signals by the MDL principle," *IEEE Transactions on Acoustics, Speech, and Signal Processing*, vol. 37, no. 8, pp. 1190–1196, 1989.

[19] S. Shahbazpanahi, S. Valaee, and M. H. Bastani, "Distributed source localization using ESPRIT algorithm," *IEEE Trans. Signal Process.*vol. 49, no. 10, pp. 2169–2178, 2001.

[20] W. Zhang, Y. Han, M. Jin, and X.-S. Li, "An improved ESPRIT-like algorithm for coherent signals DOA estimation," *IEEE Communications Letters*, vol. 24, no. 2, pp. 339–343, 2020.

[21] J. Pan, M. Sun, Y. Wang, and X. Zhang, "An enhanced spatial smoothing technique with ESPRIT algorithm for direction of arrival estimation in coherent scenarios," *IEEE Transactions on Signal Processing*, vol. 68, pp. 3635–3643, 2020.

[22] Y. Gu and A. Leshem, "Robust adaptive beamforming based on interference covariance matrix reconstruction and steering vector estimation," *IEEE Transactions on Signal Processing*, vol. 60, no. 7, pp. 3881–3885, 2012.

[23] J. Yang, J. Lu, X. Liu, and G. Liao, "Robust null broadening beamforming based on covariance matrix reconstruction via virtual interference sources," *Sensors*, vol. 20, no. 7, pp. 1865–1875, 2020.

[24] M. Grant, S. Boyd, and Y. Ye, *CVX: Matlab Software for Disciplined Convex Programming, Version 2.1*, CVX Research, Inc., Austin, TX, USA, 2017, http://cvxr.com/cvx.

[25] Y. Gu, N. A. Goodman, S. Hong, and Y. Li, "Robust adaptive beamforming based on interference covariance matrix sparse reconstruction," *Signal Processing*, vol. 96, pp. 375–381, 2014.

[26] Z. Zheng, T. Yang, W. Q. Wang, and S. Zhang, "Robust adaptive beamforming via coprime coarray interpolation," *Signal Processing*, vol. 169, Article ID 107382, 2020.

[27] R. C. Heimiller, J. E. Belyea, and P. G. Tomlinson, "Distributed array radar," *IEEE Transactions on Aerospace and Electronic Systems*, vol. AES-19, no. 6, pp. 831–839, 1983.

[28] B. Steinberg, "Phase synchronizing a nonrigid, distributed, transmit-receive radar antenna array," *IEEE Transactions on Aerospace and Electronic Systems*, vol. AES-18, no. 5, pp. 609–620, 1982.

[29] S. A. Vorobyov, A. B. Gershman, and Z.-Q. Luo, "Robust adaptive beamforming using worst-case performance optimization: a solution to the signal mismatch problem," *IEEE Transactions on Signal Processing*, vol. 51, no. 2, pp. 313–324, 2003.

[30] H. Huang, B. Liao, X. Wang, and J. Huang, "A new nested array configuration with increased degrees of freedom," *IEEE Access*, vol. 6, pp. 1490–1497, 2018.

[31] Z. Zheng, Y. Zheng, W.-Q. Wang, and H. Zhang, "Covariance matrix reconstruction with interference steering vector and power estimation for robust adaptive beamforming," *IEEE Transactions on Vehicular Technology*, vol. 67, no. 9, pp. 8495–8503, 2018.